

Elsevier instructions for the preparation of a 1-column format camera-ready paper in L^AT_EX

P. de Groot^{a*}, R. de Maas^{a†}, X.-Y. Wang^b and A. Sheffield^{a‡}

^aMathematics and Computer Science Section, Elsevier Science B.V.,
P.O. Box 103, 1000 AC Amsterdam, The Netherlands

^bEconomics Department, University of Winchester,
2 Finch Road, Winchester, Hampshire P3L T19, United Kingdom

These pages provide you with an example of the layout and style which we wish you to adopt during the preparation of your paper. Your text will be photographically reduced by 20–25%. This is the output from the L^AT_EX document class you requested.

1. FORMAT

Text should be produced within the dimensions shown on these pages: total width of 16 cm and a maximum length of 21 cm on first pages and 23 cm on second and following pages. The L^AT_EX document class uses the maximum stipulated length apart from the following two exceptions (i) L^AT_EX does not begin a new section directly at the bottom of a page, but transfers the heading to the top of the next page; (ii) L^AT_EX never (well, hardly ever) exceeds the length of the text area in order to complete a section of text or a paragraph. Here are some references: [1,2].

1.1. Spacing

We normally recommend the use of 1.0 (single) line spacing. However, when typing complicated mathematical text L^AT_EX automatically increases the space between text lines in order to prevent sub- and superscript fonts overlapping one another and making your printed matter illegible.

1.2. Fonts

These instructions have been produced using a 12 point Computer Modern Roman. Other recommended fonts are 12 point Times Roman, New Century Schoolbook, Bookman Light and Palatino.

*Footnotes should appear on the first page only to indicate your present address (if different from your normal address), research grant, sponsoring agency, etc. These are obtained with the \thanks command.

†For following authors with the same address use the \addressmark command.

‡To reuse an addressmark later on, label the address with an optional argument to the \address command, e.g. \address[MCSD], and repeat the label as the optional argument to the \addressmark command, e.g. \addressmark[MCSD].

2. PRINTOUT

The most suitable printer is a laser or an inkjet printer. A dot matrix printer should only be used if it possesses an 18 or 24 pin printhead (“letter-quality”).

The printout submitted should be an original; a photocopy is not acceptable. Please make use of good quality plain white A4 (or US Letter) paper size. *The dimensions shown here should be strictly adhered to: do not make changes to these dimensions, which are determined by the document class.* The document class leaves at least 3 cm at the top of the page before the head, which contains the page number.

Printers sometimes produce text which contains light and dark streaks, or has considerable lighting variation either between left-hand and right-hand margins or between text heads and bottoms. To achieve optimal reproduction quality, the contrast of text lettering must be uniform, sharp and dark over the whole page and throughout the article.

If corrections are made to the text, print completely new replacement pages. The contrast on these pages should be consistent with the rest of the paper as should text dimensions and font sizes.

3. TABLES AND ILLUSTRATIONS

Tables should be made with L^AT_EX; illustrations should be originals or sharp prints. They should be arranged throughout the text and preferably be included *on the same page as they are first discussed*. They should have a self-contained caption and be positioned in flush-left alignment with the text margin. Two small illustrations may be placed alongside one another as shown with Figures 1 and 2. All illustrations will undergo the same reduction as the text.

3.1. Tables

Tables should be presented in the form shown in Table 1. Their layout should be consistent throughout.

Table 1
The next-to-leading order (NLO) results *without* the pion field.

Λ (MeV)	140	150	175	200
r_d (fm)	1.973	1.972	1.974	1.978
Q_d (fm ²)	0.259	0.268	0.287	0.302
P_D (%)	2.32	2.83	4.34	6.14
μ_d	0.867	0.864	0.855	0.845
\mathcal{M}_{M1} (fm)	3.995	3.989	3.973	3.955
\mathcal{M}_{GT} (fm)	4.887	4.881	4.864	4.846
δ_{1B}^{VP} (%)	-0.45	-0.45	-0.45	-0.45
$\delta_{1B}^{C2:C}$ (%)	0.03	0.03	0.03	0.03
$\delta_{1B}^{C2:N}$ (%)	-0.19	-0.19	-0.18	-0.15

The experimental values are given in ref. [4].

Horizontal lines should be placed above and below table headings, above the subheadings and at the end of the table above any notes. Vertical lines should be avoided.

If a table is too long to fit onto one page, the table number and headings should be repeated above the continuation of the table. For this you have to reset the table counter with `\addtocounter{table}{-1}`. Alternatively, the table can be turned by 90° ('landscape mode') and spread over two consecutive pages (first an even-numbered, then an odd-numbered one) created by means of `\begin{table}[h]` without a caption. To do this, you prepare the table as a separate L^AT_EX document and attach the tables to the empty pages with a few spots of suitable glue.

3.2. Useful table packages

Modern L^AT_EX comes with several packages for tables that provide additional functionality. Below we mention a few. See the documentation of the individual packages for more details. The packages can be found in L^AT_EX's `tools` directory.

array Various extensions to L^AT_EX's `array` and `tabular` environments.

longtable Automatically break tables over several pages. Put the table in the `longtable` environment instead of the `table` environment.

dcolumn Define your own type of column. Among others, this is one way to obtain alignment on the decimal point.

tabularx Smart column width calculation within a specified table width.

rotating Print a page with a wide table or figure in landscape orientation using the `sidewaystable` or `sidewaysfigure` environments, and many other rotating tricks. Use the package with the `figuresright` option to make all tables and figures rotate in clockwise. Use the starred form of the `sideways` environments to obtain full-width tables or figures in a two-column article.

3.3. Line drawings

Line drawings may consist of laser-printed graphics or professionally drawn figures attached to the manuscript page, correctly aligned. They should be placed either at the bottom or at the top of the page. In the latter case the top of the figure should be at the same level as the first text line.

All notations and lettering should be no less than 2.5 mm high. The use of heavy black, bold lettering should be avoided as this will look unpleasantly dark when printed. Do not use too light or too dark *shading* in your figures. The pages will be reduced to 75–80% of their present size; too dark a shading may become too dense while a very light shading made of tiny points may fade away during reproduction.

3.4. PostScript figures

Instead of providing separate drawings or prints of the figures you may also use PostScript files which are included into your L^AT_EX file and printed together with the text. Use one of the packages from L^AT_EX's `graphics` directory: `graphics`, `graphicx` or `epsfig`, with the `\usepackage` command, and then use the appropriate commands (`\includegraphics` or `\epsfig`) to include your PostScript file.

Table 2: The next-to-leading order (NLO) results *without* the pion field.

Λ (MeV)	140	150	175	200	225	250	Exp.	v_{18} [?]
r_d (fm)	1.973	1.972	1.974	1.978	1.983	1.987	1.966(7)	1.967
Q_d (fm ²)	0.259	0.268	0.287	0.302	0.312	0.319	0.286	0.270
P_D (%)	2.32	2.83	4.34	6.14	8.09	9.90	—	5.76
μ_d	0.867	0.864	0.855	0.845	0.834	0.823	0.8574	0.847
\mathcal{M}_{M1} (fm)	3.995	3.989	3.973	3.955	3.936	3.918	—	3.979
\mathcal{M}_{GT} (fm)	4.887	4.881	4.864	4.846	4.827	4.810	—	4.859
δ_{1B}^{VP} (%)	-0.45	-0.45	-0.45	-0.45	-0.45	-0.44	—	-0.45
$\delta_{1B}^{C2:C}$ (%)	0.03	0.03	0.03	0.03	0.03	0.03	—	0.03
$\delta_{1B}^{C2:N}$ (%)	-0.19	-0.19	-0.18	-0.15	-0.12	-0.10	—	-0.21

The experimental values are given in ref. [4].

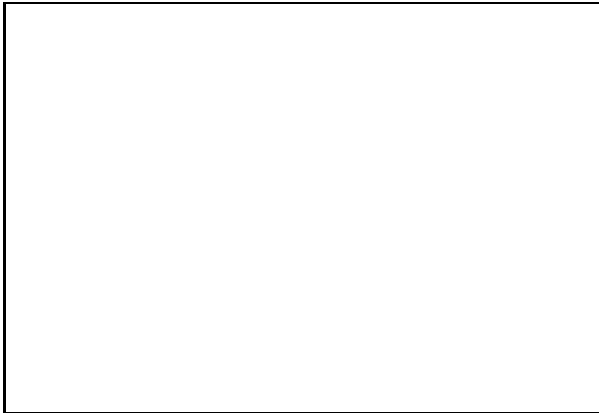


Figure 1. Good sharp prints should be used and not (distorted) photocopies.

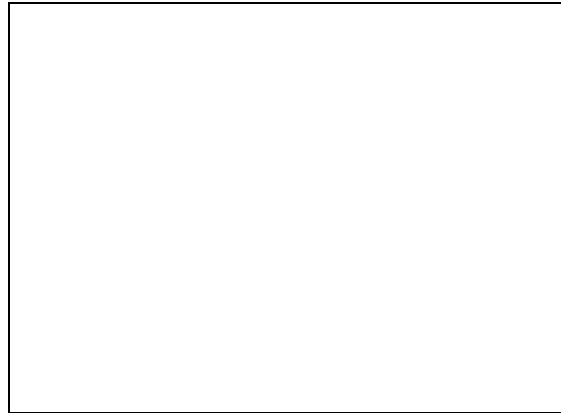


Figure 2. Remember to keep details clear and large enough to withstand a 20–25% reduction.

The simplest command is: `\includegraphics{file}`, which inserts the PostScript file `file` at its own size. The starred version of this command: `\includegraphics*{file}`, does the same, but clips the figure to its bounding box.

With the `graphicx` package one may specify a series of options as a key–value list, e.g.:

```
\includegraphics[width=15pc]{file}
\includegraphics[height=5pc]{file}
\includegraphics[scale=0.6]{file}
\includegraphics[angle=90,width=20pc]{file}
```

See the file `grfguide`, section “Including Graphics Files” of the `graphics` distribution for all options and a detailed description.

The `epsfig` package mimicks the commands familiar from the package with the same name in L^AT_EX2.09. A PostScript file `file` is included with the command
`\psfig{file=file}`.

Grey-scale and colour photographs cannot be included in this way, since reproduction from the printed CRC article would give insufficient typographical quality. See the following subsections.

3.5. Black and white photographs

Photographs must always be sharp originals (*not screened versions*) and rich in contrast. They will undergo the same reduction as the text and should be pasted on your page in the same way as line drawings.

3.6. Colour photographs

Sharp originals (*not transparencies or slides*) should be submitted close to the size expected in publication. Charges for the processing and printing of colour will be passed on to the author(s) of the paper. As costs involved are per page, care should be taken in the selection of size and shape so that two or more illustrations may be fitted together on one page. Please contact the Author Support Department at Elsevier (E-mail:

`authorsupport@elsevier.nl`) for a price quotation and layout instructions before producing your paper in its final form.

4. EQUATIONS

Equations should be flush-left with the text margin; L^AT_EX ensures that the equation is preceded and followed by one line of white space. L^AT_EX provides the document class option `fleqn` to get the flush-left effect.

$$H_{\alpha\beta}(\omega) = E_{\alpha}^{(0)}(\omega)\delta_{\alpha\beta} + \langle\alpha|W_{\pi}|\beta\rangle \quad (1)$$

You need not put in equation numbers, since this is taken care of automatically. The equation numbers are always consecutive and are printed in parentheses flush with the right-hand margin of the text and level with the last line of the equation. For multi-line equations, use the `eqnarray` environment.

For complex mathematics, use the *AMSmath* package. This package sets the math indentation to a positive value. To keep the equations flush left, either load the `espcrc` package *after* the *AMSmath* package or set the command `\mathindent=0pt` in the preamble of your article.

REFERENCES

1. S. Scholes, Discuss. Faraday Soc. No. 50 (1970) 222.
2. O.V. Mazurin and E.A. Porai-Koshits (eds.), Phase Separation in Glass, North-Holland, Amsterdam, 1984.
3. Y. Dimitriev and E. Kashchieva, J. Mater. Sci. 10 (1975) 1419.
4. D.L. Eaton, Porous Glass Support Material, US Patent No. 3 904 422 (1975).

References should be collected at the end of your paper. Do not begin them on a new page unless this is absolutely necessary. They should be prepared according to the sequential numeric system making sure that all material mentioned is generally available to the reader. Use `\cite` to refer to the entries in the bibliography so that your accumulated list corresponds to the citations made in the text body.

Above we have listed some references according to the sequential numeric system [1–4].

Abstract

We discuss the status of a subset of penetrating probes in relativistic nuclear collisions. Thermal photons and dileptons are considered, as well as the electromagnetic signature of jets.

1 Introduction

The study of penetrating probes constitutes a key aspect of the relativistic heavy ion program. In the hadronic sector, jet quenching, for example, has been a striking revelation, and has contributed to expose the qualitatively different physics that appeared in the transition from the SPS to RHIC. In this context, electromagnetic radiation also defines a privileged class of observables owing mainly to the absence of final state interactions. We briefly review some recent developments in the measurement of low- and intermediate-mass lepton pairs, and then address real photon measurements at RHIC, together with the observed suppression in the hard parton spectrum.

2 Lepton pairs

2.1 Low invariant masses

At SPS energies, the measurement of low-mass lepton pairs had previously been made by the Helios/3 [1] and by the CERES [2] experimental collaborations. As a reminder of the potential of such measurements for the discovery of new physics, it is useful to write the emission rate of lepton pairs from a finite-temperature interacting system. It is [5]

$$E_+ E_- \frac{d^6 R_{\ell^+ \ell^-}}{d^3 p_+ d^3 p_-} = \frac{2e^2}{(2\pi)^6} \frac{n_B(E, T)}{M^4} L^{\mu\nu} \text{Im} \Pi_{\mu\nu}^R \quad (1)$$

where n_B is a Bose-Einstein distribution function, $L^{\mu\nu}$ is a lepton tensor, and $\text{Im} \Pi_{\mu\nu}^R$ is the imaginary part of the in-medium, retarded, finite-temperature self-energy of the photon. Furthermore, in the nonperturbative sector, Vector Meson Dominance (VMD) relates the photon self-energy to the in-medium vector spectral density. It is therefore clear that the measurement of the low-mass spectrum of lepton pairs can reveal pristine features of the interacting many-body system. In this regard, the situation before this conference was

summarized in a presentation of the CERES collaboration [2], where three theoretical approaches were shown to be consistent with the data. Those were (i) a many-body calculation where the in-medium spectral densities are altered owing to their coupling with a variety of states accessed through interactions with a hot and dense hadronic ensemble [6]; (ii) An effective chiral model, where strong precursor effects already manifest themselves in a shifting of hadronic masses at intermediate baryonic densities [7]; (iii) A simple thermal parametrization of the quark-antiquark annihilation Born rates, justified by a duality argument [8]. Finally and importantly, approaches solely based on vacuum properties have difficulty providing an interpretation of the CERES measurements.

It is probably fair to write that one of the highlights of the Quark Matter 2005 meeting has been the disclosure of the new NA60 data [3] for In-In collisions at the CERN SPS. The low-mass dilepton component of this experiment's measurements is of exceptional quality and statistics [3, 4]. The experimental collaboration also has shown a comparison with their data with the results of approaches (i) and (ii), above. On the basis of that comparison, the experimental data strongly suggest that large mass shifts of the vector mesons are not observed. This same comparison also shows consistency with the many-body calculations of (i) above. An immediate conclusion is the following: NA60 data are now precise enough to distinguish between different approaches, or at least between some of the more extreme scenarios. This is important progress, and represents a great stride forward. Whether this rules out or not entire classes of models will remain to be seen, but one point is clear: the approach shown by the experimental collaboration which is based on in-medium mass shifts *is the same one that was in agreement with CERES results* [6]. It is entirely possible that theoretical refinements are needed in order to be in line with evolving theoretical paradigms, but the fact remains that any single theory now has to deal with two separate experimental results.

The low-mass results do signal an unambiguous many-body effect. To go beyond this to a state of deeper theoretical understanding is not an easy task. For example, one of the original aims of this whole experimental program was to isolate a signal (precursor or not) of chiral symmetry restoration. This goal has unfortunately remained elusive, owing largely to the difficulty of directly extracting an axialvector correlator from relativistic heavy ion data. In the chiral limit, vector and axialvector correlators are constrained by sum rules of the Weinberg-type [9], and these may be realized in several different ways

[10]. The ability to chart a path to correlator degeneracy (in the Weinberg sense) would definitely represent a significant breakthrough. However, the precise data shown at this meeting will surely fuel many investigations.

2.2 Intermediate invariant masses

The study of lepton pair production at intermediate masses ($m_\phi < M < m_{J/\psi}$) are especially interesting in the context of searches for the quark-gluon plasma, as kinematical arguments combined with the original high temperature of the QCD plasma would designate the intermediate invariant mass region as a window of opportunity for the observation of plasma radiation [11, 12]. In this context, considerable interest was generated by the fact that an excess over sources expected from pA measurements has been confirmed in the intermediate mass region by the Helios/3 [1] and NA50 [16] collaborations. This excess could in turn signal an increase in $c\bar{c}$ abundances, which would then manifest itself through the correlated semileptonic decays of open charm mesons. Alternatively, thermal lepton pairs need to be ruled out as viable scenario before other explanations be invoked. Those thermal sources are akin to the ones identified in the low dilepton mass sector by the many-body calculations. Showing that they also shine at higher invariant masses would go a long way in providing a consistent picture of electromagnetic radiation in heavy ion collisions. In the theoretical interpretation of such data, a potential caveat is lurking, and is related to the use of effective Lagrangian techniques. These rely on physical parameters which were essentially all fitted in regions characterized by soft energy scales, and had mostly to do with strong and electromagnetic decay widths. When moving over to larger invariant masses, off-shell effects will set in, making controlled extrapolations a problem [13]. Fortunately, there exists a wealth of data of the type $e^+e^- \rightarrow \text{hadrons}$, which cover precisely the same range in invariant mass as the heavy ion data [14]. These data can be analyzed channel-by-channel and have been used, together with τ -decay measurements, to construct the vector and axial vector spectral densities that can be related to the lepton pair spectrum [15]. Summing all kinematically-relevant channels, one arrives at a source which may be compared to the data via the space-time modeling of the nuclear collision. The result of one such exercise is shown in Figure 1. It is fair to write that the specific values of the temperature evolution, for example, depend somewhat on the particularities of the space-time modeling. However, a fairly robust conclusion still emerges: the intermediate-mass

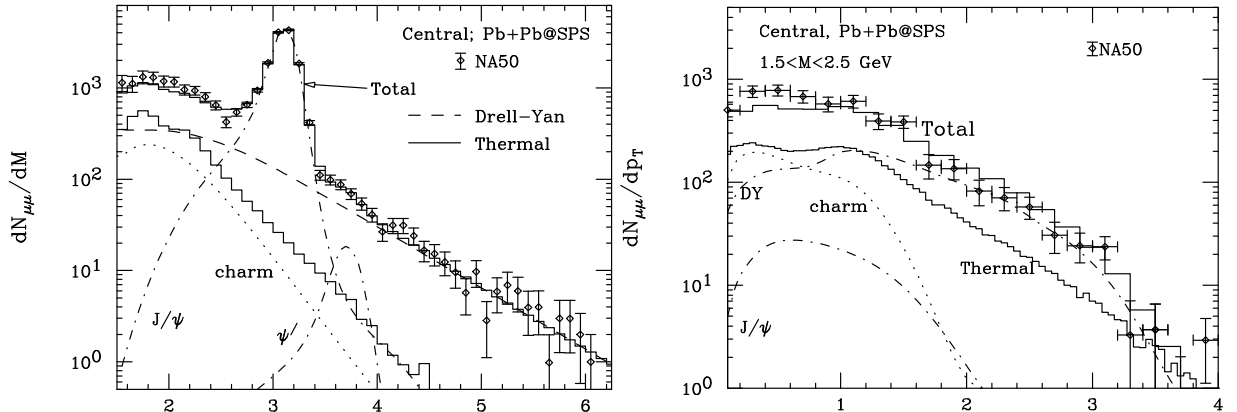


Figure 1: The invariant mass and momentum spectra, calculated for $\mu\mu$ pairs, calculated for $\mu\mu$ pairs. The sources are Drell-Yan, correlated charm decay, and thermal (quark-gluon plasma and hadron gas). The full curve histogram is the sum of all of those different contributions, after correcting for detector acceptance, resolution, and efficiency.

NA50 data does not demand a large contribution from plasma radiation (it is about 20% here), nor does it need a large enhancement of the initial charm content. Even though specific details do differ, this conclusion is shared by other theoretical studies of a similar nature [17, 18, 19]. However, in order to bring this situation to some degree of closure, a direct measurement of the strangeness component would go a long way. This has now been done and has been reported at this conference by the NA60 collaboration [3, 20]. The first measures taken by the collaboration was to experimentally confirm the presence of an enhancement in the intermediate-mass continuum in nuclear collisions, over what is seen in proton-nucleus events. However, with the new information provided by the muon offset measurement, NA60 can now assert that the excess is not linked with open charm enhancement. This new data is also compatible with the excess that had previously been observed by NA50. The analysis will proceed further, but it already reveals that the signal that exceeds what is associated with pA sources increases faster than linearly with the number of participants. The statistics will improve, the 2004 proton-nucleus data will be analyzed and such measurements are important for the determination of QCD effects beyond leading-twist [22]. It is however clear that these results do represent a great leap in our quest for a complete quantitative understanding of the electromagnetic radiation being produced in relativistic nuclear collisions.

3 Photons from jet-plasma interactions

One of the most striking findings of the RHIC program is the strong apparent modification of jet characteristics, following a passage through an interacting, dense medium [21]. A compelling theoretical interpretation of these results is that of jet absorption, signaling in effect the existence of a hot and dense partonic phase. Several models of jet-quenching through gluon bremsstrahlung have been elaborated [23, 24, 25, 26, 27]. Here, we use that of AMY [28], because of its potential to handle consistently jet energy loss and photon emission. In this approach, Fokker-Planck equations are solved to obtain the time-evolution of the initial hard gluon, $P_g(p, t = 0)$ and hard quark plus antiquark distributions, $P_{q\bar{q}}(p, t = 0)$. The coupled equations are

$$\begin{aligned} \frac{dP_{q\bar{q}}(p)}{dt} &= \int_k P_{q\bar{q}}(p + k) \frac{d\Gamma_{qg}^q(p + k, k)}{dkdt} - P_{q\bar{q}}(p) \frac{d\Gamma_{qg}^q(p, k)}{dkdt} + 2P_g(p + k) \frac{d\Gamma_{q\bar{q}}^g(p + k, k)}{dkdt} \\ \frac{dP_g(p)}{dt} &= \int_k P_{q\bar{q}}(p + k) \frac{d\Gamma_{qg}^q(p + k, p)}{dkdt} + P_g(p + k) \frac{d\Gamma_{gg}^g(p + k, k)}{dkdt} \\ &\quad - P_g(p) \left(\frac{d\Gamma_{q\bar{q}}^g(p, k)}{dkdt} + \frac{d\Gamma_{gg}^g(p, k)}{dkdt} \Theta(2k - p) \right) \end{aligned} \quad (2)$$

The kernels $d\Gamma(p, k)/dkdt$ are the transition rates, and they contain the resummation effects typical of interactions with a thermal medium [28]. The solution of the joint equations for the time-evolution of the parton distribution functions permits the modeling in real time of the partonic spectra. The hard parton can then fragment into the different varieties of observed particles. Up to suppressed corrections, the cross section for produced pions in nucleon-nucleon collisions can be written in a factorized form as

$$\frac{d^3\sigma_{pp}}{d^2p_\perp dy} = \sum_{a,b,c,d} \int dx_a dx_b g(x_a, Q) g(x_b, Q) K_{\text{jet}} \frac{d\sigma^{a+b \rightarrow c+d}}{dt} \frac{1}{\pi z} D_{\pi^0/c}(z, Q') , \quad (3)$$

where $g(x, Q)$ is the parton distribution function in a nucleon, $D_{\pi^0/c}$ is the pion fragmentation function, $d\sigma^{ab \rightarrow cd}/dt$ is the parton-parton cross section at leading order, and K_{jet} accounts for higher order effects. Here, “jet” essentially means a fast parton with $p_T \gg 1$ GeV. This procedure, with the factorization scale (Q) and the fragmentation scale (Q') set equal to p_T , the CTEQ5 parton distribution functions, and $K_{\text{jet}} \sim 1.7$, does a very good job of reproducing the measured π^0 above $p_T \approx 5$ GeV [29], in nucleon-nucleon collisions at RHIC. This is shown in Figure 2.

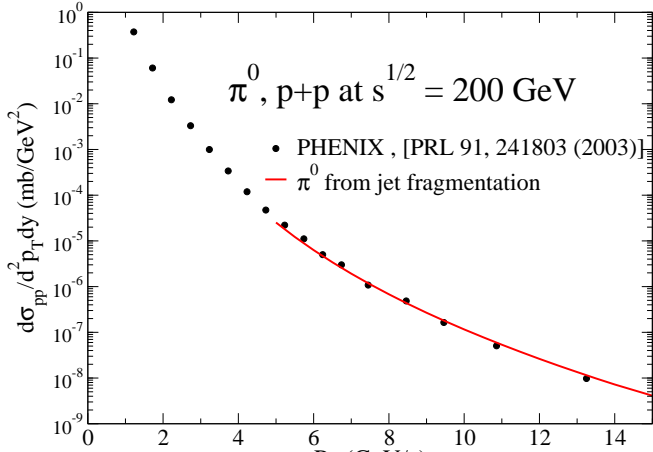


Figure 2: Neutral pion spectra in pp collisions at RHIC. The data points are from PHENIX, and the calculated results are from jet fragmentation.

To obtain the high p_T π^0 cross section in AA collisions, the pp calculation must be modified in two important ways. First, the parton distribution function of a nucleus differs from that of a proton:

$$g_A(x_a, Q) = g(x_a, Q)R_A(x_a, Q) \quad (4)$$

The nuclear modification factor of the structure function R_A takes into account shadowing and anti-shadowing [30]. Also, the hard parton loses energy between the initial hard scattering and its hadronization, and this information is contained in the time-evolution of the entire partonic profile we have described earlier. The π^0 spectrum obtained in AA collisions is then

$$\frac{d^3 N_{AA}}{dy d^2 p_T} = \frac{\langle N_{coll} \rangle}{\sigma_{in}} \sum_{a,b,c,d} \int dx_a dx_b g_A(x_a, Q) g_A(x_b, Q) K_{jet} \frac{d\sigma^{a+b \rightarrow c+d}}{dt} \frac{\tilde{D}_{\pi^0/a}(z, Q)}{\pi z} \quad (5)$$

where $\langle N_{coll} \rangle$ is the average number of binary collisions, σ_{in} is the inelastic nucleon-nucleon cross section, and the medium-modified fragmentation function is

$$\tilde{D}_{\pi^0/c}(z, Q) = \int d^2 r_\perp \mathcal{P}(\mathbf{r}_\perp) \tilde{D}_{\pi^0/c}(z, Q, \mathbf{r}_\perp, \mathbf{n}) \quad (6)$$

where \mathcal{P} takes into account the geometry of the emitting source, and

$$\tilde{D}_{\pi^0/c}(z, Q, \mathbf{r}, \mathbf{n}) = \int dp_f \frac{z'}{z} \left(P_{q\bar{q}/c}(p_f; p_i) D_{\pi^0/q}(z', Q) + P_{g/c}(p_f; p_i) D_{\pi^0/g}(z', Q) \right) \quad (7)$$

where $z = p_T/p_i$, and $z' = p_T/p_f$. Note also that $P_{q\bar{q}/c}(p_f; p_i)$ and $P_{g/c}(p_f; p_i)$ are the solutions to the Fokker-Planck equation and represent the probability to get a given parton with final momentum p_f , given that the initial configuration is a particle of type c and momentum p_i . Information on the initial temperature sensitivity, on the geometry and other details is in Ref. [29].

A quantitative measure of in-medium modifications is contained in the so-called R_{AA} profile

$$R_{AA} = \frac{\sigma_{\text{in}} d^3 N_{AA} / dy d^2 p_T}{\langle N_{\text{coll}} \rangle d^3 \sigma_{pp} / dy d^2 p_T}, \quad (8)$$

when plotted as a function of the transverse momentum. Clearly, if a nucleus-nucleus collision is nothing but a superposition of nucleon-nucleon collisions, then R_{AA} should be unity. This variable is now available for a variety of particles, over a wide range of transverse momenta. Figure 3 reveals new

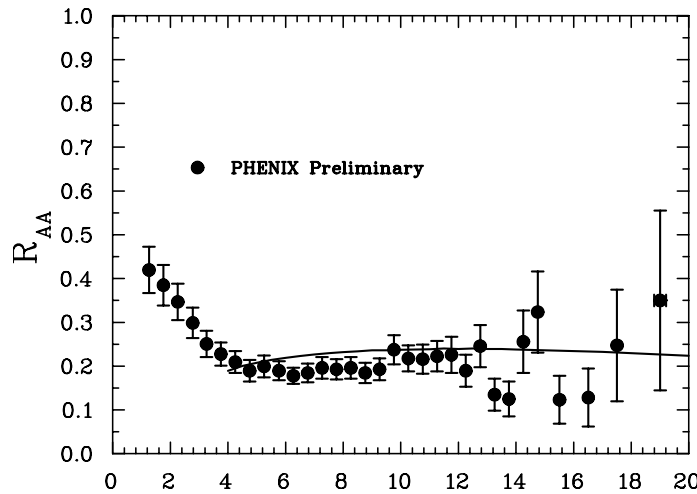


Figure 3: The ratio R_{AA} for π^0 , as a function of transverse momentum. The full line is the calculation described in this text, and in [29], with $\alpha_s = 0.34$. The initial temperature is 370 MeV, and is consistent with the study in [31]. Data are from [32].

preliminary data, where the behavior of R_{AA} over an impressive range of almost 20 GeV/c is shown. Also there, is the result of a calculation with the formalism described here. In this approach, the strong coupling constant, α_s , is a free parameter. In his plot, a value of $\alpha_s = 0.34$ yields a good fit. This value is kept fixed for the rest of this work. Further note there are uncertainties associated with the determination of $\langle N_{\text{coll}} \rangle$, as well as

inherent systematic measurement uncertainties. This combination roughly is of the order of 10%. The apparent agreement (for $p_T \geq 4$ GeV) is at least superficially satisfying, even if many questions remain on details of the opacity of the medium, and on the actual sensitivity of this variable on bulk properties. The answer to those questions is at present scheme-dependent. With data of this quality however, the next meeting in this series is bound to see progress on these issues. Nevertheless, the flatness of these spectra appears a robust feature. The softer part of the spectrum is not reproduced by a QCD fragmentation framework and requires additional ingredients possibly related to parton recombination [33].

With the machinery at hand, the spectrum of photons produced in nucleus-nucleus collisions can be calculated, including those originating for jet-plasma interactions [34], but consistently taking account energy-loss systematics. The sources include those active in pp collisions: the direct photons produced by parton Compton and annihilation events, and the fragmentation photons produced by bremsstrahlung from final state partons. In AA collisions, the sources above still operate but the fragmenting jets are now subject to energy-loss considerations. In addition, hard partons traveling in the medium can also produce photons through medium-induced bremsstrahlung. Finally, the conversion of leading partons to photons [34, 29] was found to be a significant contribution and should be treated consistently with the other channels enumerated here. The different sources for Au + Au collisions at RHIC are shown in Figure 4. The agreement with the recent PHENIX photon data is very good. Furthermore, it is satisfying to note that the modeling parameters were fixed prior to its release [29]. Further note that when the jet-photon conversions are omitted, the total photon production is reduced by up to 45% around $p_T = 3$ GeV/c, showing the importance of this process. The total plasma contribution appears important for $p_T < 6$ GeV/c. Here also, the quality of this data opens the door to additional investigations. Some have been done [36] and more will follow, but importantly, electromagnetic signals and hard hadronic probes are no longer disjoint observables.

4 Conclusion

It is not an overstatement to write that the measurement of electromagnetic probes in relativistic has produced some very exciting results. All expectations are that this will continue, with larger statistics samples and the

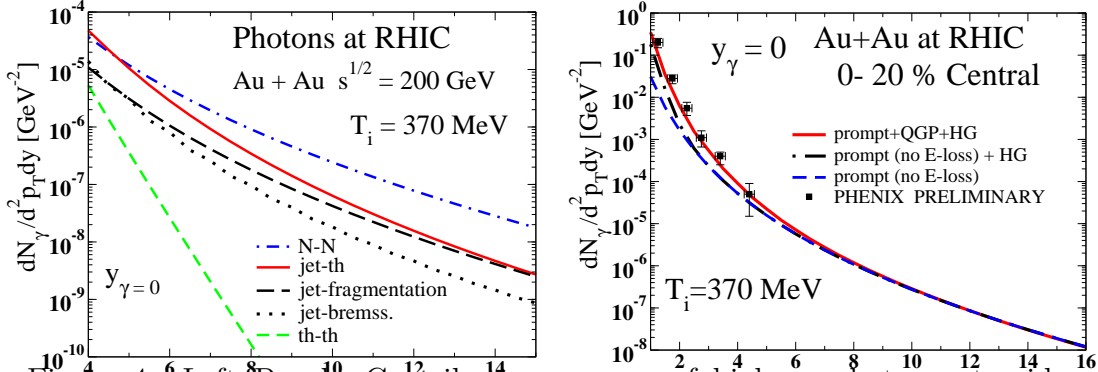


Figure 4: Left Panel: Contributing sources of high- p_T photons at mid-rapidity in central nuclear collisions at RHIC. Solid line: jet-photon conversion in the plasma; dotted line: bremsstrahlung from jets in the plasma; short dashed line: thermal photons [31]; long dashed line: photons from fragmenting jets; dot-dashed line: contribution from the primordial hard scattering. Right panel: Total production of photons at RHIC, compared with new PHENIX data [35]. The solid line represents all processes from the left panel together with photons from the hadronic gas (HG) [31]; the dot-dashed line do not include any plasma-related contributions but has those from the HG. Photons from pp collisions scaled to AA are shown by the dashed lines. measurement of lepton pairs at RHIC. With the data shown at this meeting, we are entering an era of precision measurements and modeling. For example, measurements of photon azimuthal asymmetry are now at reach.

Acknowledgments

I am grateful to all of my collaborators for their involvement with any aspect of the work presented here. Of those, I also thank Simon Turbide for a critical reading of this manuscript. This work was supported in part by the Natural Sciences and Engineering Research Council of Canada, and in part by the Fonds Nature et Technologies of the Government of Quebec.

References

[1] M. A. Mazoni *et al.*, Nucl. Phys. **A566** (1994) 95c; M. Masera *et al.*, Nucl. Phys. **A590** (1995) 93c; A. L. S. Angelis *et al.*, Eur. Phys. J. C **13** (2000) 433.

- [2] D. Miśkowiec, these proceedings.
- [3] E. Scomparin, these proceedings
- [4] S. Damjanovic, these proceedings.
- [5] H. A. Weldon, Phys. Rev. D **42** (1990) 2384; Charles Gale and Joseph I. Kapusta, Nucl. Phys. **B357** (1991) 65.
- [6] R. Rapp and J. Wambach, Adv. Nucl. Phys. **25** (2000) 1.
- [7] See, for example, G. E. brown and Mannque Rho, Phys. Rep. **363** (2002) 85.
- [8] K. Gallmeister *et al.*, Nucl. Phys. **A715** (2003) 705.
- [9] S. Weinberg, Phys. Rev. Lett. **18** (1987) 507.
- [10] J. I. Kapusta and E. V. Shuryak, Phys. Rev. D **49** 46944704 (1994).
- [11] E. V. Shuryak, Phys. Lett. B **78** (1978) 150.
- [12] K. Kajantie, J. Kapusta, L. McLerran, and A. Mekjian, Phys. Rev. D **34** (1986) 2746.
- [13] S. Gao and C. Gale, Phys. Rev. C **57** (1998) 254.
- [14] See, for example, S. I. Dolinsky *et al.*, Phys. Rep. **202** (1991) 99, and references therein.
- [15] Z. Huang, Phys. Lett. B **361** (1995) 131, and private communication.
- [16] M. C. Abreu *et al.*, Eur. Phys. J. C **14** (2000) 443.
- [17] G. Q. Li and C. Gale, Phys. Rev. Lett. **81** (1998) 1572; Phys. Rev. C **58** (1998) 2914.
- [18] R. Rapp and E. V. Shuryak, Phys. Lett. B **473** (2000) 13.
- [19] K. Gallmeister, B. Kämpfer, and O. P. Pavlenko, Phys. Lett. B **473** (2000) 20.
- [20] R. Shahoyan, these proceedings.

- [21] X.-N. Wang, these proceedings.
- [22] See, for example, Jan-Wei Qiu, Eur. Phys. J. C **43** (2005) 239.
- [23] R. Baier, Y. L. Dokshitzer, A. H. Mueller, S. Peigné, and D. Schiff, Nucl. Phys. **B484** (1997) 291; R. Baier, Y. L. Dokshitzer, A. H. Mueller, and D. Schiff, JHEP **0109** (2001) 33.
- [24] E. Wang and X.-N. Wang, Phys. Rev. Lett. **89** (2002) 162301.
- [25] I. Vitev and M. Gyulassy, Phys. Rev. Lett. **89** (2002) 252301.
- [26] A. Kovner and U. A. Wiedemann, *QGP3*, R. Hwa and X.-N. Wang, editors (World Scientific, Singapore, 2003).
- [27] B. G. Zakharov, JETP lett. **63** (1996) 952; *ibid.* **65** (1997) 615; *ibid.* **70** (1999) 176.
- [28] P. Arnold, G. D. Moore, and L. G. Yaffe, JHEP **0111** (2001) 57; JHEP **0206** (2002) 30.
- [29] S. Turbide, C. Gale, S. Jeon, and G. D. Moore, Phys. Rev. C **72**, 014906 (2005).
- [30] K. J. Eskola, V. J. Kolhinen, and C. A. Salgado, Eur. Phys. J. C **9**, 61 (1999).
- [31] S. Turbide, R. Rapp, and C. Gale, Phys. Rev. C **69**, 014903 (2004).
- [32] B. Cole, these proceedings.
- [33] D. Molnár, these proceedings.
- [34] R. J. Fries, B. Müller, and D. K. Srivastava, Phys. Rev. Lett. **90**, 132301 (2003).
- [35] H. Buesching, these proceedings.
- [36] D. d'Enterria and D. Peressounko, nucl-th/0503003.